Atmos. Chem. Phys. Discuss., 14, 29209–29236, 2014
www.atmos-chem-phys-discuss.net/14/29209/2014/
doi:10.5194/acpd-14-29209-2014

Atmospheric Chemistry and Physics Discussions

The impact of temperature resolution on trajectory modeling of stratospheric water vapour

T. Wang[1,2], A. E. Dessler[1], M. R. Schoeberl[3], W. J. Randel[4], and J.-E. Kim[5]

[1]Texas A&M University, College Station, Texas, USA
[2]NASA Jet Propulsion Laboratory/California Institute of Technology, Pasadena, California, USA
[3]Science and Technology Corporation, Columbia, Maryland, USA
[4]National Center for Atmospheric Research, Boulder, Colorado, USA
[5]University of Colorado, Boulder, Colorado, USA

Received: 28 September 2014 – Accepted: 31 October 2014 – Published: 24 November 2014

Correspondence to: T. Wang (tao.wang@jpl.nasa.gov)

Published by Copernicus Publications on behalf of the European Geosciences Union.

Abstract

Lagrangian trajectories driven by reanalysis meteorological fields are frequently used to study water vapour (H_2O) in the stratosphere, in which the tropical cold-point temperatures regulate H_2O amount entering the stratosphere. Therefore, the accuracy of temperatures in the tropical tropopause layer (TTL) is of great importance for trajectory studies. Currently, most reanalyses, such as the NASA MERRA (Modern Era Retrospective-Analysis for Research and Applications), only provide temperatures with ~ 1.2 km vertical resolution in the TTL, which has been argued to introduce uncertainties in the simulations. In this paper, we quantify this uncertainty by comparing the trajectory results using MERRA temperatures on model levels (traj.MER-T) to those using temperatures in finite resolutions, including GPS temperatures (traj.GPS-T) and MERRA temperatures adjusted to recover wave-induced variability underrepresented by the current ~ 1.2 km vertical resolution (traj.MER-Twave). Comparing with traj.MER-T, traj.GPS-T has little impact on simulated stratospheric H_2O (changes ~ 0.1 ppmv), whereas traj.MER-Twave tends to dry air by 0.2–0.3 ppmv. The bimodal dehydration peaks in traj.MER-T due to limited vertical resolution disappear in traj.GPS-T and traj.MER-Twave by allowing the cold-point tropopause to be found at finer vertical levels. Despite these differences in absolute values of predicted H_2O and vertical dehydration patterns, there is virtually no difference in the interannual variability in different runs. Overall, we find that the finite resolution of temperature has limited impact on predicted H_2O in the trajectory model.

1 Introduction

Stratospheric water vapour (H_2O) and its feedback play an important role in regulating the global radiation budget and the climate system (e.g., Holton et al., 1995; Randel et al., 2006; Solomon et al., 2010; Dessler et al., 2013). It has been known since Brewer's seminal work on stratospheric circulation that tropical tropopause tempera-

ACPD
14, 29209–29236, 2014

ture is the main driver of stratospheric H_2O concentration (Brewer, 1949). As parcels approach and pass through the cold-point tropopause – the altitude at which air temperature is coldest, condensation occurs, thereby regulating the parcel's H_2O concentration to local saturation level (e.g., Fueglistaler et al., 2009, and references therein). This is the dehydration process. The role of tropopause temperature variation in dehydration is most apparent in the annual variation in tropical stratospheric H_2O, also known as the "tape recorder" (Mote et al., 1996).

When air enters the TTL, due to encounter of lower temperatures it experiences multiple dehydrations, and the final stratospheric H_2O mixing ratio is established after air passing through the coldest temperature, which sets the strong relation between cold-point tropopause and the entry level H_2O (e.g., Holton and Gettelman, 2001; Randel et al., 2004, 2006).

The details of the transport and dehydration process can be understood by performing Lagrangian trajectory simulations, which track the temperature history of a large number of individual parcels. Unlike simulating chemical tracers that depends strongly on the transport imposed (Ploeger et al., 2011; Wang et al., 2014), the simulation of H_2O is primarily constrained by tropopause temperatures. Dehydration thus primarily depends on the air parcel temperature history; so stratospheric H_2O simulations ultimately require accurate analyses of temperatures (e.g., Mote et al., 1996; Fueglistaler et al., 2005, 2009; Liu et al., 2010; Schoeberl and Dessler, 2011; Schoeberl et al., 2012, 2013).

In this paper, we use a forward, domain-filling trajectory model to study the detailed dehydration behavior of air parcels and the carrying H_2O in the lower stratosphere. Previous analyses (Schoeberl and Dessler, 2011; Schoeberl et al., 2012, 2013) have demonstrated that this model can accurately simulate many of the aspects of the observed stratospheric H_2O distributions. Despite the good agreements, there are clear areas of uncertainty, such as the accuracy of circulation fields (Schoeberl et al., 2012), the detailed dehydration mechanisms (Schoeberl et al., 2014), the impacts from convection (Schoeberl et al., 2011, 2014), and the resolution of temperatures in the TTL,

ACPD
14, 29209–29236, 2014

etc. In this paper, we investigate uncertainties introduced by the last one – the effect of vertical resolution of temperatures.

We will examine the impact of the relatively coarse vertical resolution of reanalysis temperature on trajectory simulations of stratospheric H_2O and the dehydration patterns. This is accomplished by comparing trajectory results from using NASA Modern Era Retrospective-Analysis for Research and Applications (MERRA) (Rienecker et al., 2011) temperatures in model levels, to using GPS temperatures and the MERRA temperatures adjusted to account for resolved but underrepresented waves (Kim and Alexander, 2013), both in finer vertical resolution. This will help us to further understand the dehydration of air entering the stratosphere.

2 Trajectory model and temperatures used

2.1 Trajectory model

The trajectory model used here follows the details described in Schoeberl and Dessler (2011) with trajectories calculated using the Bowman trajectory code (Bowman, 1993; Bowman et al., 2013). This model has been proven to be able to simulate both H_2O (Schoeberl and Dessler, 2011; Schoeberl et al., 2012, 2013) and chemical tracers (Wang et al., 2014) in the lower stratosphere very well. Because of the overly dispersive behavior of kinematic trajectories (e.g., Schoeberl et al., 2003; Liu et al., 2010; Ploeger et al., 2010; Schoeberl and Dessler, 2011), we perform diabatic trajectories using isentropic coordinates, in which the vertical velocity is the potential temperature tendency converted from the diabatic heating rates via the thermodynamic equation (e.g., Andrews et al., 1987).

The parcel initiation level is chosen to be the 370 K isentrope, which is above the level of zero radiative heating (~ 355–365 K, Gettelman and Forster, 2002) and below the tropical tropopause (~ 375–380 K) in the tropics. Every day, parcels are initialized on equal area grids covering 40° N–40° S and advected forward in time by reanaly-

ACPD
14, 29209–29236, 2014

sis winds. At the end of each day, any parcel that has descended below the 345 K (~ 250 hPa or ~ 10 km) level is removed since in most cases they have re-entered the troposphere. The upper boundary is chosen to be 2200 K isentrope (~ 1 hPa or ~ 50 km) to cover the entire stratosphere. Parcels are initialized and added to the ensemble consecutively and the combined set of parcels is then advected forward. This process is repeated over the entire integration period so that after 2–3 years the stratospheric domain is filled up with parcels – this is the concept of domain-filling that guarantees robust statistics.

H_2O is conserved along the trajectories, except when saturation occurs then excess of H_2O is instantaneously removed from the parcel to keep the relative humidity with respect to ice from exceeding 100 %. This is sometimes referred as "instant dehydration" (e.g., Schoeberl et al., 2014). This simple scheme that ignores detailed microphysics has been proven to be able to simulate many features of H_2O in the lower stratosphere (e.g., Fueglistaler et al., 2005; Jensen and Pfister, 2004; Gettelman et al., 2002).

For each parcel, we also consider the H_2O oxidized from the carrying methane. As described in Schoeberl and Dessler (2011), we use photochemical loss rates supplied from Goddard two-dimensional stratospheric chemistry model (Fleming et al., 2007) to photolyze each methane molecule into two molecules of H_2O (Dessler et al., 1994). Noted that all results in this paper are limited in the tropical 110–50 hPa, where methane oxidation has little impacts on total H_2O abundances (refer Fig. 6 in Schoeberl et al., 2012).

Along each trajectory, we locate the point when air experiences minimum saturation mixing ratio as the final dehydration point (FDP), which determines the final stratospheric H_2O mixing ratio for that trajectory. The saturation mixing ratio associated with this point is referred as FDP-H_2O.

2.2 Temperature datasets

In this paper, we use MERRA (Rienecker et al., 2011) circulation to advect the parcels. This includes horizontal wind components and total diabatic heating rates from all sky.

ACPD
14, 29209–29236, 2014

As shown in Schoeberl et al. (2012, 2013), trajectory model driven by this reanalysis yields excellent estimates of H_2O compared to observations by the Aura Microwave Limb Sounder (MLS) (Read et al., 2007).

Driven by the same circulation, we use three different temperature datasets to quantify the uncertainty induced by temperature vertical resolutions: (1) MERRA temperatures on model levels, denoted as *traj.MER-T*; (2) GPS radio occultation (RO) temperatures, denoted as *traj.GPS-T*; and (3) MERRA temperatures adjusted to include waves that are not represented well in current coarse model levels (Kim and Alexander, 2013), denoted as *traj.MER-Twave*. Different from earlier papers that uses an idealized parameterizations of waves added to the temperature datasets (e.g., Schoeberl and Dessler, 2011), here we amplify waves that are underrepresented in the coarse vertical resolution of MERRA temperatures. Note that MERRA does not assimilate GPS observations, which makes the two temperature datasets independent from each other. Trajectory runs with the three different temperature datasets are summarized in Table 1.

2.2.1 GPS temperature

Owing to its high vertical resolution, GPS temperature profiles capture the cold-point tropopause in unprecedented accuracy. In this paper we use GPS wet profile (wetPrf) retrieved at 100 m vertical resolution from a one-dimensional variational technique based on ECMWF analysis. The wetPrf and GPS Atmospheric Profile (atmPrf, derived assuming no water vapor in the air) temperatures are essentially the same in 200–10 hPa but below 200 hPa the errors in atmPrf could be as high as ~ 3 K due to neglect of water vapour (Das and Pan, 2014). Despite being retrieved at 100 m resolution, the actual vertical resolution of GPS profiles ranges from 0.5 km in the lower troposphere to ~ 1 km in the middle atmosphere (Kursinski et al., 1997).

The GPS radio occultation (RO) technique makes the data accuracy independent of platforms. It has been reported that the biases among different RO payloads could be as low as 0.2 K in the UTLS (Ho et al., 2009). Therefore, to compensate the relatively lower horizontal resolution (relative to that of reanalysis), we include GPS RO

ACPD
14, 29209–29236, 2014

from all platforms, which include the Constellation Observing System for Meteorology, Ionosphere, and Climate (COSMIC) (Anthes et al., 2008), the CHAllenging Minisatellite Payload (CHAMP) satellite (Wickert et al., 2001), the Communications/Navigation Outage Forecasting System (CNOFS), the Gravity Recovery And Climate Experiment (GRACE) twin satellites (Beyerle et al., 2005), the Meteorological Operational Polar Satellite-A (MetOp-A), the Satellite de Aplicaciones Cientifico-C (SACC) satellite (Hajj et al., 2004), and the TerraSAR-X (TerraSAR-X). There are ∼ 3000 profiles per day, mostly from COSMIC, with ∼ 1200 profiles of these in the tropics.

Each day, GPS temperature profiles are binned to 200 m vertical resolution. Horizontally, we grid data into 2.5 × 1.25 (longitude by latitude) grids with 2-D Gaussian function weighting. We use over 7 years of GPS data available from July 2006 to December 2013, and the trajectory run using it is denoted as *traj.GPS-T*.

Figure 1 shows a snapshot of the 100 hPa GPS raw (panel a) and gridded (panel b) temperature on 1 January 2010, comparing with MERRA temperature (panel c). It demonstrates that the gridded GPS temperature clearly captures most of the variability horizontally, although some detailed structure might be lost due to its relatively sparse measurements.

Figure 2 shows the GPS and MERRA temperature differences (GPS–MERRA) averaged over the deep tropics (18° S–18° N) during the GPS period. Here, we examine the differences at the MERRA model levels (black dots) as well as MERRA in-between levels (grey dots), which are obtained by linearly interpolating both GPS and MERRA temperature to the same pressure levels. Here we use linear instead of higher order, such as cubic, interpolation because linear scheme performs better (see Sect. 2.2.3). Apparently, within the TTL GPS temperatures are warmer at MERRA model levels, but in-between the MERRA levels GPS temperatures are colder (as much as ∼ 0.4 K) around the cold-point tropopause (generally between 100 and 85 hPa), which would bring at most 0.4 ppmv dry bias in the entry level of stratospheric H_2O assuming 100 % saturation.

ACPD
14, 29209–29236, 2014

2.2.2 MERRA temperature adjusted by waves

Waves are underrepresented in reanalyses, therefore a further interpolation in the vertical significantly dampens even resolved waves due to relatively coarse vertical resolution (as seen in comparisons with high resolution radiosondes; Kim and Alexander, 2013). To overcome these limitations, a new wave scheme was developed by Kim and Alexander (2013) to recover the underrepresented variability, based on amplitude-phase interpolation and amplification of waves in reanalysis datasets.

For each month's MERRA temperature profiles, we construct a 90 day time series at each level centered on that month. Then the Fourier transformation is applied on the time series to obtain amplitudes and phases in frequency domain. Those amplitude and phase profiles in real space are then interpolated separately into finer 200 m vertical levels to bring back the variability induced by waves. After reconstructing new complex functions from the interpolated amplitudes and phases, amplification factors for the four seasons are applied to enhance wave variability since waves are already weaker at reanalysis levels. The amplification factors are defined as the fractional differences between the square roots of power spectra in reanalysis and radiosonde data. Finally, the inverse Fourier transformation is applied to bring the time series back to the time domain. Applying this scheme on MERRA temperature records yields a new MERRA temperature dataset that has realistic variability induced by waves (Kim and Alexander, 2013) and the trajectory model performed on this temperature is denoted as *traj.MERTwave*.

The wave scheme produces both positive and negative perturbations to the MERRA temperature profiles, depending on the phase of waves. Overall, the change in temperature induced by waves is less than 2 K (Fig. 3), although in rare cases it can reach 5–7 K. Importantly, however, about 80 % of the changes in cold-point temperature are negative, with the wave scheme lowering the average cold-point temperatures by ~ 0.35 K. It is this reduction in cold-point temperature that is responsible for the reduction in H_2O entering the stratosphere.

ACPD
14, 29209–29236, 2014

2.2.3 Interpolation scheme

For all three trajectory runs, we use linear interpolation in calculating the temperature of parcels. Due to the strong curvature of temperature profiles around the cold-point tropopause, some previous analyses have used higher order interpolations, such as cubic spline (e.g., Liu et al., 2010), to make assumptions about the curly nature of temperature profile.

In order to determine if linear or cubic spline interpolation is superior, we sample GPS tropical temperature profiles at MERRA vertical levels and then use the two interpolation schemes to reconstruct the full GPS resolution. Then we compare the minimum saturation mixing ratio from the recovered profiles to the minimum calculated from the full resolution GPS profiles. Figure 4a shows the probability distribution of the differences between the minimum saturation mixing ratio in the full-resolution GPS profile and in the two interpolation schemes. On average, the linear interpolation performs better (RMS difference is 0.18 and 0.25 ppmv for the linear and cubic spline, respectively). Figure 4b shows the corresponding probability distribution of the difference of the pressure of this minimum, and the linear interpolation does better for this metric, too (RMS difference is 5.2 and 7.2 hPa for the linear and the cubic spline interpolation, respectively). We have also tested higher order spline interpolations and find that none produce lower RMS errors than linear interpolation. Overall, cubic spline interpolation tends to underestimate cold-point temperature (sometimes unrealistically to as low as ~ 150 K), making the implied H_2O too dry, as noted by Liu et al. (2010).

3 Trajectory results

3.1 Dehydration patterns

The gridded GPS temperatures are available since July 2006, so for fair comparison we start all trajectory runs at that time and run them forward till the end of 2013. For each

ACPD
14, 29209–29236, 2014

model run, we calculate statistics of the final dehydration points (FDP) for all parcels entering the stratosphere. We define "parcels entering the stratosphere" as parcels that underwent final dehydration between 45° N–45° S (thus ignoring polar dehydration) and that were at altitudes higher (pressure lower) than 90 hPa six months after their FDP event. Averaging over 7 years minimizes the effects of interannual variability.

Figure 5 compares the FDP frequency and the FDP saturation mixing ratio (FDP-H_2O) among three runs. In all cases, it is clear that dehydration occurs almost exclusively between 60 and 110 hPa. The dashed lines represent the average FDP-H_2O, which reaches a minimum at 85 hPa for all runs, meaning parcels dehydrated in its vicinity carry the smallest amount of H_2O into the stratosphere. The relatively high FDP-H_2O above 80 hPa (just above the entry level) comes from the parcels that avoided the tropical cold trap and experienced final dehydration at higher, warmer levels of the stratosphere. Out of ~ 1.3 millions of parcels in the stratosphere there are only ~ 0.3 % bypassed the cold-point tropopause, and these parcels have little impact on the stratosphere.

The FDP frequency, however, shows large differences among the runs. The run using MERRA temperature (*traj.MER-T*) yields a bimodal FDP maxima distinctly at ~ 98 and ~ 84 hPa, close to the MERRA model levels (100.5 and 85.4 hPa), respectively. This occurs because the cold-point tropopause is constrained to be near these two levels due to limited vertical resolution in MERRA temperature, whereas in real atmosphere it may fall in between (see Fig. 7 below). The dehydration profiles implied from using the other two datasets, however, have a more gradual variation of cold-point altitude, with maximum occurring midway between the MERRA levels.

Figure 6 depicts the vertical distributions of normalized FDP in time (panel a–c) and longitude (panel d–f) for the three different runs. We see that the MERRA coarse model levels do not capture the variations of cold-point tropopause well during MAM (March-April-May) and SON (September-October-November), resulting in discontinuous transition of FDP from DJF (December-January-February) to MAM, and from JJA (June-July-August) to SON (panel a). When using GPS temperatures (panel b) and MERRA

ACPD
14, 29209–29236, 2014

temperatures adjusted to amplify underrepresented waves (panel c), the dehydration patterns show continuous variations throughout the year. Take the SON for example, the longitudinal distribution of dehydration patterns emphasizes the bi-modal feature of using MERRA temperature (panel d) contradictory to the single mode feature of using GPS temperature (panel e) or MERRA temperature adjusted by waves (panel f), with enhancements centered at 85 and 98 hPa corresponding to the altitudes of most frequent cold-point tropopause during DJF and JJA, respectively.

The FDP seasonal changes follow exactly the variations of the cold-point tropopause represented differently by the three temperature records. During SON, for example, Fig. 7 shows that the cold-point tropopause in GPS temperatures (panel a, red) or MERRA temperature adjusted by waves (panel a, blue) can be found most frequently within 100–85 hPa in this season. Trajectory runs therefore yield peak FDP occurring at the same level (panel b red and blue lines). However, due to lacking of levels between 100 and 85 hPa in MERRA temperatures, the cold-point tropopause is pushed to one of the two closest levels (panel a black bars), resulting in bimodal FDP distributions (panel b black line) and is therefore responsible for the discontinuity in FDP shown in Fig. 6a and d. The same argument applies to the MAM results, too. During DJF and JJA, however, the cold-point tropopause is close to a particular level (DJF to 85 hPa and JJA to 100 hPa, not shown here), generating a single, prominent dehydration peak.

3.2 Water Vapour (H_2O)

It is obvious that trajectory simulations using GPS temperatures (*traj.GPS-T*) and MERRA temperatures adjusted by waves (*traj.MER-Twave*) tend to yield more reasonable FDP patterns around the cold-point tropopause (Fig. 5 solid lines), although the parcels dehydrated at a particular altitude have a similar amount of water vapour in all three models (FDP H_2O, Fig. 5 dashed lines). A more interesting question is whether the different dehydration occurrences affect the stratospheric H_2O predicted by the trajectory model.

ACPD
14, 29209–29236, 2014

Figure 8 compares the tropical (18° N–18° S) H_2O profile predicted from three trajectory runs. Here, we compare results from *traj.MER-Twave* and *traj.GPS-T* to the results from *traj.MER-T* to see the differences induced by waves and by using GPS temperatures. We see slightly drier air in GPS run expected since GPS temperatures are at most ~ 0.4 K lower than that of MERRA around the tropopause (Fig. 2); whereas waves yield air 0.2–0.3 ppmv drier, in agreement with previous calculations (e.g., Jensen et al., 2004; Schoeberl et al., 2011).

Figure 8b also shows that comparing to *traj.MER-T*, the dry biases from using GPS temperatures are largest in MAM and SON (0.14–0.21 ppmv on average, red curves), when the cold-point tropopause is between the MERRA's 100.5 and 85.4 hPa standard levels. During DJF and JJA, when the cold point is near one of the two MERRA standard levels, the differences become smaller. Thus we conclude that using GPS temperatures in finite vertical resolution decreases simulated stratospheric H_2O by an average of ~ 0.1 ppmv, accounting for ~ 2.5 % given typical stratospheric H_2O abundances of 4 ppmv.

It is important to point out that, despite these differences in the absolute value of H_2O, there is virtually no difference in the anomalies (remainder after subtracting the average annual cycle). In Fig. 9a we compare the time series of H_2O anomaly at 83 hPa from three different trajectory runs weighted by the MLS averaging kernels as well the MLS observations. Note that the interannual variations of approximately ±0.5 ppmv in H_2O are in good agreement with the year-to-year changes of about ±1 K in cold-point tropopause temperatures (Fig. 9b) for all three different runs, further supports the knowledge that the two are strongly coupled (e.g., Randel et al., 2004, 2006; Randel and Jensen, 2013). Clearly, for studying the interannual variability of H_2O, MERRA temperatures in coarse vertical resolution are as good as temperatures in higher vertical resolution.

ACPD
14, 29209–29236, 2014

4 Summary

The domain-filling, forward trajectory model is a useful tool in examining the processes controlling the water vapour (H_2O) entering the stratospheric. In the model, the dehydration of air entering the stratosphere largely depends on the cold-point temperature around the tropopause, which may not be represented accurately by reanalyses due to their relatively coarse vertical resolution.

To investigate the impacts of under-represented cold-point temperatures, we compare trajectory results from using MERRA model-level temperatures to those using temperature datasets in finer vertical resolution. This includes GPS temperatures and an adjusted MERRA temperature dataset that uses a wave scheme developed by Kim and Alexander (2013) to reconstruct underrepresented vertical variability in MERRA temperatures.

Compared with using MERRA original temperatures, we find that using higher resolution GPS temperatures dries the stratosphere by ~ 0.1 ppmv, and using MERRA temperatures adjusted with waves dries the stratosphere by ~ 0.2–0.3 ppmv. This is consistent with previous analyses (e.g., Jensen et al., 2004; Schoeberl et al., 2011). Despite the predicted differences in H_2O abundances, the interannual variability (the residual after subtracting the mean annual cycle) exhibits virtually no differences, due to the strong coupling between stratospheric H_2O and tropical cold-point temperatures. Therefore, in terms of studying the interannual changes of stratospheric H_2O, we argue that reanalysis temperatures are more useful due to its long-term availability.

Looking at the locations of FDP points, we find a bimodal distribution when using MERRA temperatures on model levels (Figs. 5–7). This is caused by the fact that the cold-point is constrained to be near the two MERRA model levels (100.5 and 85.4 hPa) that bracket the cold-point tropopause (Fig. 7a, black histograms). When using the temperature fields with higher vertical resolution, the resultant FDP patterns appear to be more physically reasonable (Figs. 5–7).

ACPD
14, 29209–29236, 2014

In this paper we perform linear interpolations for all trajectory runs. Other analyses have used cubic spline interpolation owing to the strong curvature of temperature profile around the cold-point tropopause. We investigate the performances of both schemes using GPS temperature profiles (Sect. 2.2.3) and find that while introducing new information due to its assumption in the temperature profile around the tropopause, cubic spline scheme tends to generate unrealistically low cold-point temperature due to cubic fitting. Therefore, the results are not necessarily realistic and on the other hand linear interpolation is overall more accurate (Fig. 4).

It is well-known that trajectory models can accurately simulate stratospheric humidity, despite obvious problems (e.g., resolution of the cold-point temperature, dehydration mechanisms, lack of convection, supersaturation, etc.). In this paper, we have investigated one of these – the effect of vertical resolution – and find that it is comparatively minor. This provides some confidence that the trajectory model driven by current modern reanalyses is useful in depicting the stratospheric water vapour in the long run.

Acknowledgements. The authors thank Kenneth Bowman, Joan Alexander, and Eric Jensen for their helpful discussions and comments. This work was supported by NSF AGS-1261948, NASA grant NNX13AK25G and NNX14AF15G, and partially under the NASA Aura Science Program. This work was partially carried out during visits of Tao Wang funded by the Graduate Student Visitor Program under the Advanced Study Program (ASP) at the National Center for Atmospheric Research (NCAR), which is operated by the University Corporation for Atmospheric Research, under sponsorship of the National Science Foundation.

References

Andrews, D. G., Holton, J. R., and Leovy, C. B.: Middle Atmosphere Dynamics, Academic Press, Orlando, Florida, 489 pp., 1987.

Anthes, R. A., Bernhardt, P. A., Chen, Y., Cucurull, L., Dymond, K. F., Ector, D., Healy, S. B., Ho, S.-P., Hunt, D. C., Kuo, Y.-H., Liu, H., Manning, K., McCormick, C., Meehan, T. K., Randel, W. J., Rocken, C., Schreiner, W. S., Sokolovskiy, S. V., Syndergaard, S., Thompson, D. C.,

ACPD
14, 29209–29236, 2014

Trenberth, K. E., Wee, T.-K., Yen, N. L., and Zeng, Z.: The COSMIC/FORMOSAT-3 Mission: Early Results, B. Am. Meteorol. Soc., 89, 313–333, doi:10.1175/BAMS-89-3-313, 2008.
Beyerle, G., Schmidt, T., Michalak, G., Heise, S., Wickert, J., and Reigber, C.: GPS radio occultation with GRACE: atmospheric profiling utilizing the zero difference technique, Geophys. Res. Lett., 32, L13806, doi:10.1029/2005GL023109, 2005.
Bowman, K. P.: Large-scale isentropic mixing properties of the Antarctic polar vortex from analyzed winds, J. Geophys. Res., 98, 23013–23027, 1993.
Bowman, K. P., Lin, J. C., Stohl, A., Draxler, R., Konopka, P., Andrews, A., and Brunner, D.: Input data requirements Lagrangian Trajectory Models, B. Am. Meteorol. Soc., 94, 1051–1058, doi:10.1175/BAMS-D-12-00076.1, 2013.
Brewer, A. W.: Evidence for a world circulation provided by the measurements of helium and water vapor distribution in the stratosphere, Q. J. Roy. Meteor. Soc., 75, 351–363, 1949.
Das, U. and Pan, C. J.: Validation of FORMOSAT-3/COSMIC level 2 "atmPrf" global temperature data in the stratosphere, Atmos. Meas. Tech., 7, 731–742, doi:10.5194/amt-7-731-2014, 2014.
Dessler, A. E., Weinstock, E. M., Hintsa, E. J., Anderson, J. G., Webster, C. R., May, R. D., Elkins, J. W., and Dutton, G. S.: An examination of the total hydrogen budget of the lower stratosphere, Geophys. Res. Lett., 21, 2563–2566, 1994.
Dessler, A. E., Schoeberl, M. R., Wang, T., Davis, S. M., and Rosenlof, K. H.: Stratospheric water vapor feedback, P. Natl. Acad. Sci. USA, 110, 18087–18091, doi:10.1073/pnas.1310344110, 2013.
Fleming, E. L., Jackman, C. H., Weisenstein, D. K., and Ko, M. K. W.: The impact of interannual variability on multidecadal total ozone simulations, J. Geophys. Res., 112, D10310, doi:10.1029/2006JD007953, 2007.
Fueglistaler, S., Bonazzola, M., Haynes, P. H., and Peter, T.: Stratospheric water vapor predicted from the Lagrangian temperature history of air entering the stratosphere in the tropics, J. Geophys. Res., 110, D08107, doi:10.1029/2004JD005516, 2005.
Fueglistaler, S., Dessler, A. E., Dunkerton, T. J., Folkins, I., Fu, Q., and Mote, P. W.: The tropical tropopause layer, Rev. Geophys., 47, RG1004, doi:10.1029/2008RG000267, 2009.
Gettelman, A. and de Forster, P. M.: Definition and climatology of the tropical tropopause layer, J. Meteorol. Soc. Jpn., 80, 911–924, 2002.
Gettelman, A., Randel, W. J., Wu, F., and Massie, S. T.: Transport of water vapor in the tropical tropopause layer, Geophys. Res. Lett., doi:10.1029/2001GL013818, 2002.

ACPD
14, 29209–29236, 2014

Hajj, G. A., Ao, C. O., Iijima, B. A., Kuang, D., Kursinski, E. R., Mannucci, A. J., Meehan, T. K., Romans, L. J., de La Torre Juarez, M., and Yunck, T. P.: CHAMP and SAC-C atmospheric occultation results and intercomparisons, J. Geophys. Res., 109, D06109, doi:10.1029/2003JD003909, 2004.

Ho, S.-P., Goldberg, M., Kuo, Y.-H., Zou, C.-Z., and Schreiner, W.: Calibration of temperature in the lower stratosphere from microwave measurements using COSMIC radio occultation data: preliminary results, Terr. Atmos. Ocean. Sci., 20, 87–100, 2009.

Holton, J. R. and Gettelman, A.: Horizontal transport and the dehydration of the stratosphere, Geophys. Res. Lett., 28, 2799–2802, doi:10.1029/2001GL013148, 2001.

Holton, J. R., Haynes, P. H., McIntyre, M. E., Douglass, A. R., Rood, R. B., and Pfister, L.: Stratosphere–troposphere exchange, Rev. Geophys., 334, 405–439, 1995.

Jensen, E. and Pfister, L.: Transport and freeze-drying in the tropical tropopause layer, J. Geophys. Res., 109, D02207, doi:10.1029/2003JD004022, 2004.

Kim, J.-E. and Alexander, J. M.: A new wave scheme for trajectory simulations of stratospheric water vapor, Geophys. Res. Lett., 40, 5286–5290, doi:10.1002/grl.50963, 2013.

Kursinski, E. R., Hajj, G. A., Schofield, J. T., Linfield, R. P., and Hardy, K. R.: Observing Earth's atmosphere with radio occultation measurements using the Global Positioning System, J. Geophys. Res., 102, 23429–23465, doi:10.1029/97JD01569, 1997.

Liu, Y. S., Fueglistaler, S., and Haynes, P. H.: Advection-condensation paradigm for stratospheric water vapor, J. Geophys. Res., 115, D24307, doi:10.1029/2010jd014352, 2010.

Mote, P. W., Rosenlof, K. H., McIntyre, M. E., Carr, E. S., Gille, J. C., Holton, J. R., Kinnersley, J. S., Pumphrey, H. C., Russell III, J. M., and Waters, J. W.: An atmospheric tape recorder: the imprint of tropical tropopause temperatures on stratospheric water vapor, J. Geophys. Res., 101, 3989–4006, 1996.

Ploeger, F., Konopka, P., Günther, G., Grooß, J.-U., and Müller, R.: Impact of the vertical velocity scheme on modeling transport across the tropical tropopause layer, J. Geophys. Res., 115, doi:10.1029/2009JD012023, 2010.

Ploeger, F., Fueglistaler, S., Grooß, J.-U., Günther, G., Konopka, P., Liu, Y. S., Müller, R., Ravegnani, F., Schiller, C., Ulanovski, A., and Riese, M.: Insight from ozone and water vapour on transport in the tropical tropopause layer (TTL), Atmos. Chem. Phys., 11, 407–419, doi:10.5194/acp-11-407-2011, 2011.

Randel, W. J. and Jensen, E. J.: Physical processes in the tropical tropopause layer and their role in a changing climate, Nat. Geosci., 6, 169–176, doi:10.1038/ngeo1733, 2013.

ACPD
14, 29209–29236, 2014

Randel, W. J., Wu, F., Oltmans, S. J., Rosenlof, K. H., and Nedoluha, G. E.: Interannual changes of stratospheric water vapor and correlations with tropical tropopause temperatures, J. Atmos. Sci., 61, 2133–2148, doi:10.1175/1520-0469(2004)061<2133:ICOSWV>2.0.CO;2, 2004.

Randel, W. J., Wu, F., Vömel, H., Nedoluha, G. E., and Forster, P.: Decreases in stratospheric water vapor after 2001: links to changes in the tropical tropopause and the Brewer–Dobson circulation, J. Geophys. Res., 111, D12312, doi:10.1029/2005JD006744, 2006.

Read, W. G., Lambert, A., Bacmeister, J., Cofield, R. E., Christensen, L. E., Cuddy, D. T., Daffer, W. H., Drouin, B. J., Fetzer, E., Froidevaux, L., Fuller, R., Herman, R., Jarnot, R. F., Jiang, J. H., Jiang, Y. B., Kelly, K., Knosp, B. W., Kovalenko, L. J., Livesey, N. J., Liu, H. C., Manney, G. L., Pickett, H. M., Pumphrey, H. C., Rosenlof, K. H., Sabounchi, X., Santee, M. L., Schwartz, M. J., Snyder, W. V., Stek, P. C., Su, H., Takacs, L. L., Thurstans, R. P., Vomel, H., Wagner, P. A., Waters, J. W., Webster, C. R., Weinstock, E. M., and Wu, D. L.: Aura Microwave Limb Sounder upper tropospheric and lower stratospheric H_2O and relative humidity with respect to ice validation, J. Geophys. Res., 112, D24S35, doi:10.1029/2007JD008752, 2007.

Rienecker, M. M., Suarez, M. J., Gelaro, R., Todling, R., Bacmeister, J., Liu, E., Bosilovich, M. G., Schubert, S. D., Takacs, L., Kim, G.-K., Bloom, S., Chen, J., Collins, D., Conaty, A., da Silva, A., Gu, W., Joiner, J., Koster, R. D., Lucchesi, R., Molod, A., Owens, T., Pawson, S., Pegion, P., Redder, C. R., Reichle, R., Robertson, F. R., Ruddick, A. G., Sienkiewicz, M., and Woollen, J.: MERRA – NASA's modern-era retrospective analysis for research and applications, J. Climate, 24, 3624–3648, doi:10.1175/JCLI-D-11-00015.1, 2011.

Schoeberl, M. R. and Dessler, A. E.: Dehydration of the stratosphere, Atmos. Chem. Phys., 11, 8433–8446, doi:10.5194/acp-11-8433-2011, 2011.

Schoeberl, M. R., Douglass, A. R., Zhu, Z. X., and Pawson, S.: A comparison of the lower stratospheric age spectra derived from a general circulation model and two data assimilation systems, J. Geophys. Res., 108, 4113, 2003.

Schoeberl, M. R., Dessler, A. E., and Wang, T.: Simulation of stratospheric water vapor and trends using three reanalyses, Atmos. Chem. Phys., 12, 6475–6487, doi:10.5194/acp-12-6475-2012, 2012.

Schoeberl, M. R., Dessler, A. E., and Wang, T.: Modeling upper tropospheric and lower stratospheric water vapor anomalies, Atmos. Chem. Phys., 13, 7783–7793, doi:10.5194/acp-13-7783-2013, 2013.

ACPD
14, 29209–29236, 2014

The impact of temperature resolution on trajectory modeling

T. Wang et al.

Schoeberl, M. R., Dessler, A. E., Wang, T., Avery, M. A, and Jensen, E.: Cloud Formation, Convection, and Stratospheric Dehydration, Earth and Space Science, doi:10.1002/2014EA000014, 2014.

Solomon, S., Rosenlof, K. H., Portmann, R. W., Daniel, J. S., Davis, S. M., Sanford, T. J., and Plattner, G.-K.: Contributions of stratospheric water vapor to decadal changes in the rate of global warming, Science, 327, 1219–1223, 2010.

Wang, T., Randel, W. J., Dessler, A. E., Schoeberl, M. R., and Kinnison, D. E.: Trajectory model simulations of ozone (O_3) and carbon monoxide (CO) in the lower stratosphere, Atmos. Chem. Phys., 14, 7135–7147, doi:10.5194/acp-14-7135-2014, 2014.

Wickert, J., Reigber, C., Beyerle, G., König, R., Marquardt, C., Schmidt, T., Grundwaldt, L., Galas, R., Meehan, T. K., Melbourne, W. G., and Hocke, K.: Atmosphere sounding by GPS radio occultation: first results from CHAMP, Geophys. Res. Lett., 28, 3263–3266, 2011.

ACPD
14, 29209–29236, 2014

Table 1. Different temperature datasets used in trajectory model.

Temperature Datasets	Availability	Horizontal Resolution (Longitude × Latitude)	Vertical Resolution In TTL	Trajectory Runs Denoted
MERRA	Daily*	2/3 × 1/2	~ 1.2 km	traj.MER-T
GPS (gridded)	Daily	2.5 × 1.25	0.2 km	traj.GPS-T
MERRA w/waves	Daily*	2/3 × 1/2	0.2 km	traj.MER-Twave

* These datasets are available 6 hourly. For fair comparison with using GPS data, we used daily averages.

ACPD
14, 29209–29236, 2014

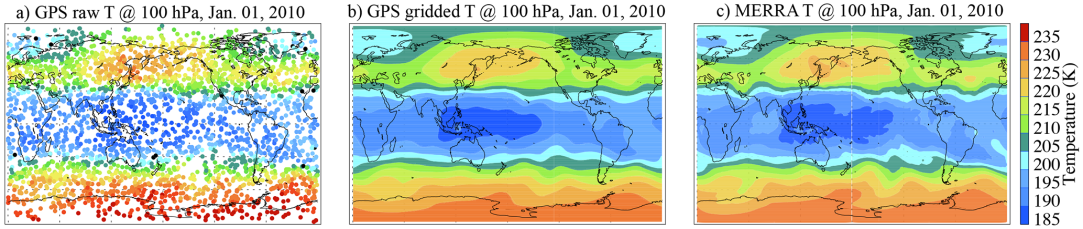

Figure 1. Comparison of temperatures from raw GPS **(a)**, gridded GPS **(b)**, and MERRA temperature **(c)** at 100 hPa on 1 January 2010.

ACPD
14, 29209–29236, 2014

The impact of temperature resolution on trajectory modeling

T. Wang et al.

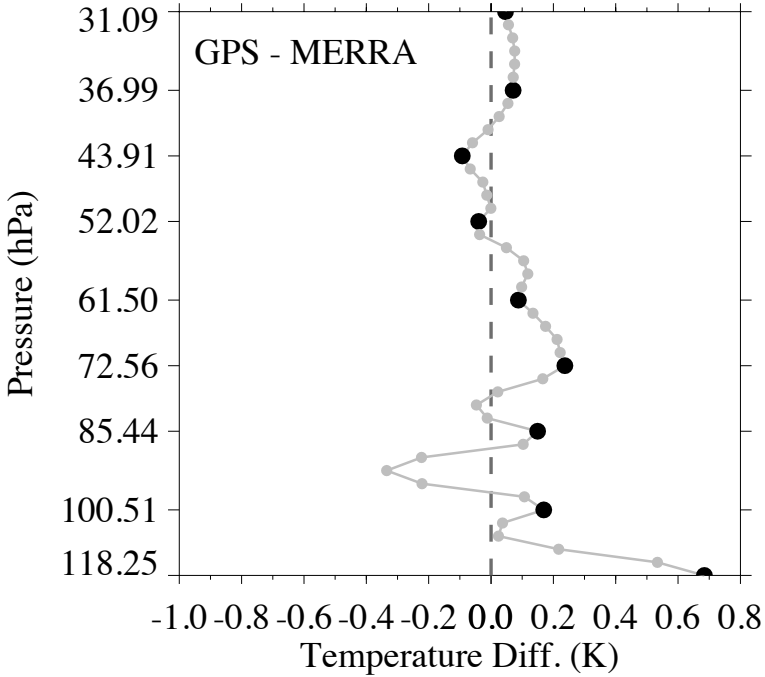

Figure 2. Temperature differences between GPS and MERRA at MERRA model levels (black dots) and MERRA in-between levels, averaged over the deep tropics (18° S–18° N) from July 2006 to December 2013. Temperature in-between MERRA levels are obtained from linear interpolation.

ACPD
14, 29209–29236, 2014

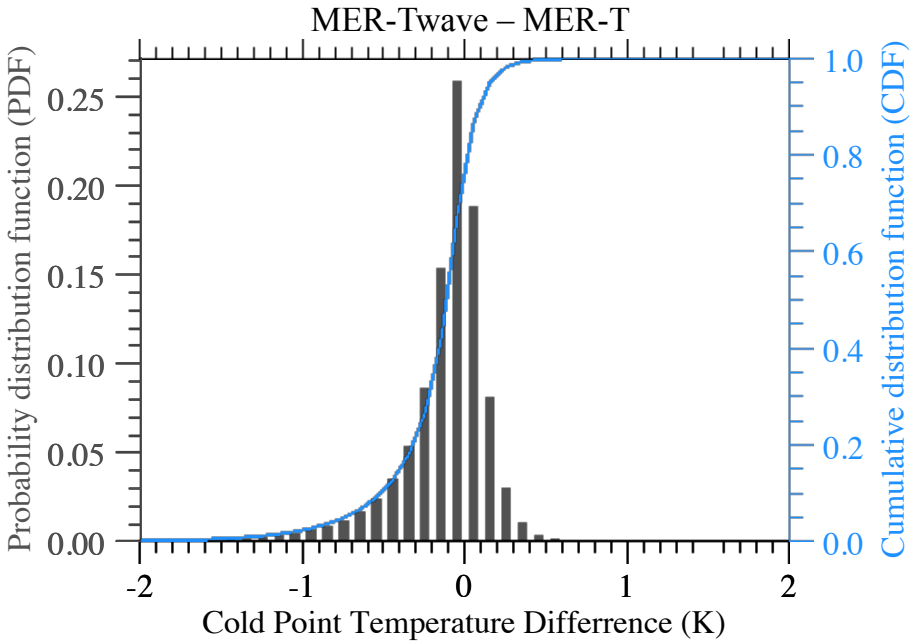

Figure 3. Cold-Point temperature differences between MERRA adjusted by waves and MERRA (MER-Twave – MER-T) during 2007–2013. The PDF in black is plotted on left *y* axis and CDF in blue on right *y* axis.

ACPD
14, 29209–29236, 2014

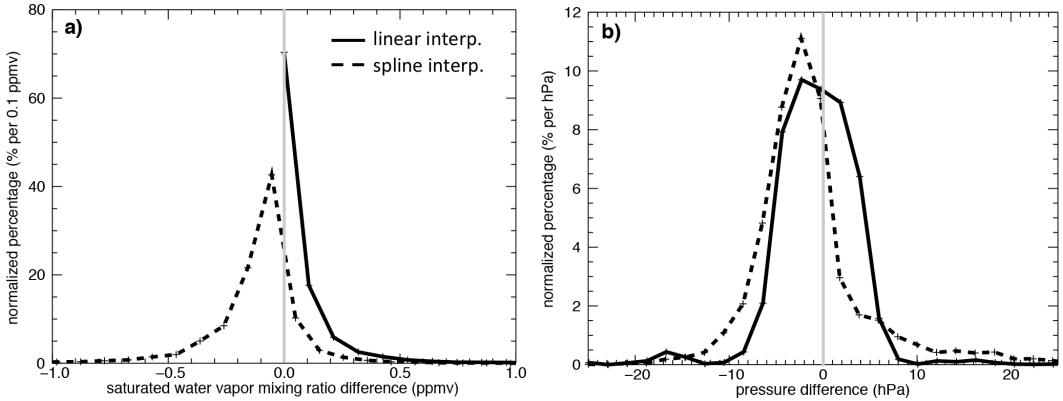

Figure 4. PDFs of the differences between linear or cubic spline interpolations to the actual value form the GPS temperature profiles. **(a)** Minimum saturation mixing ratio of the profile (units are percent per 0.1 ppmv); **(b)** pressure of the saturation mixing ratio minimum (units are percent per hPa). The plus signs in each line mark the bin intervals.

ACPD
14, 29209–29236, 2014

The impact of temperature resolution on trajectory modeling

T. Wang et al.

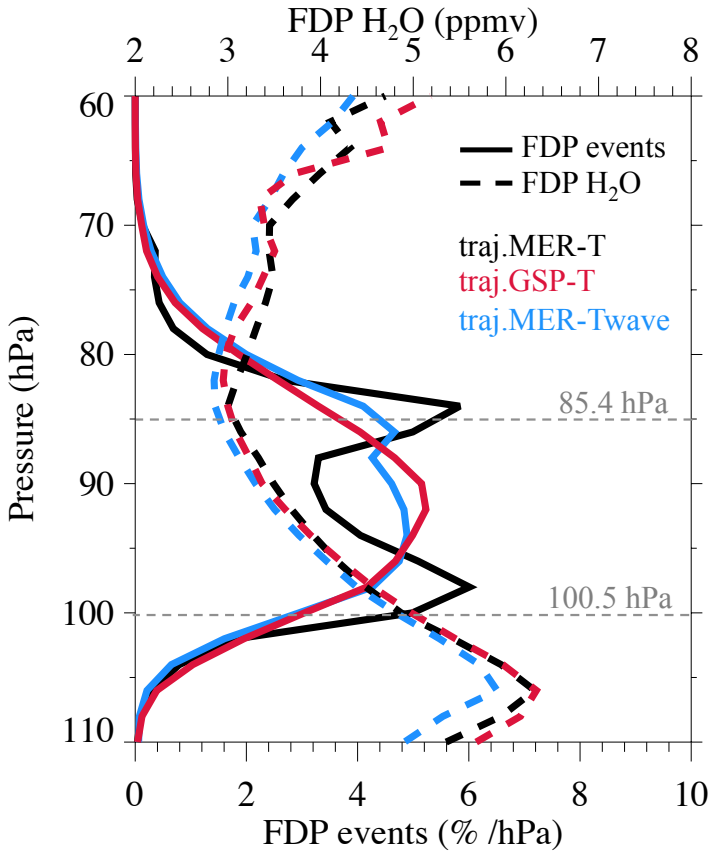

Figure 5. Annual average of vertical distributions of FDP events (in %hPa^{-1}, solid lines, lower *x* axis) and FDP saturation mixing ratios (FDP-H_2O, ppmv, dashed lines, upper *x* axis) from trajectory simulations using MERRA temperatures (black), GPS temperatures (red), and MERRA temperatures adjusted by waves (blue).

ACPD
14, 29209–29236, 2014

The impact of temperature resolution on trajectory modeling

T. Wang et al.

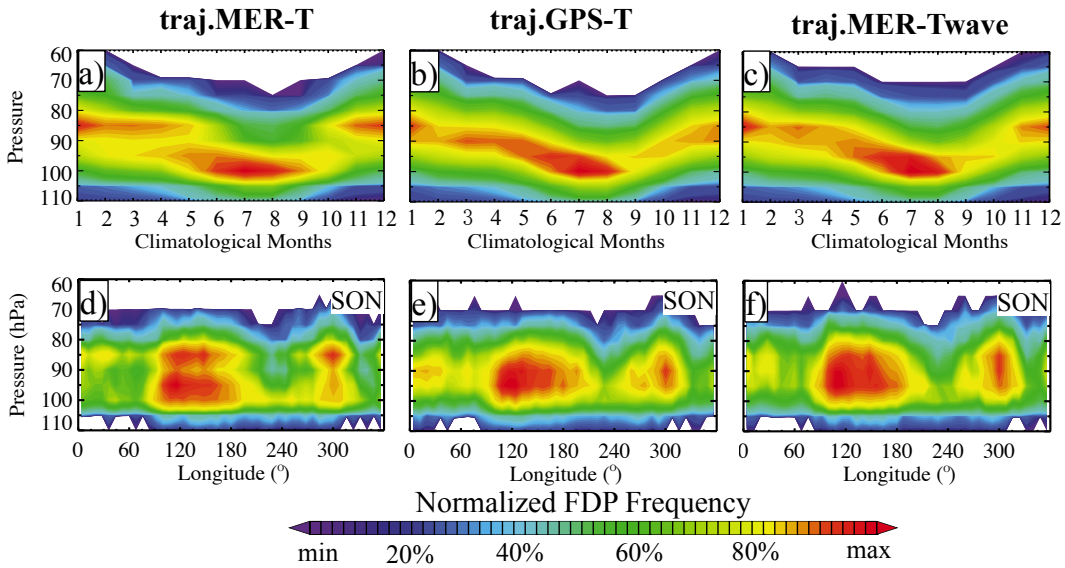

Figure 6. Vertical distributions of normalized FDP events in time-evolutional **(a–c)** views among trajectory simulations by using **(a)** MERRA temperature (*traj.MER-T*), **(b)** GPS RO temperature (*traj.GPS-T*), and **(c)** MERRA temperature adjusted by waves (*traj.MER-Twave*). The longitudinal variations of FDP during SON are highlighted in **(d–f)** to emphasize the discontinuity in FDP from *traj.MER-T*. All panels are plotted in their own range and color-coded at the same percentiles (i.e., 0, 20, 40, . . . , 100 %) to compare the patterns.

ACPD
14, 29209–29236, 2014

The impact of temperature resolution on trajectory modeling

T. Wang et al.

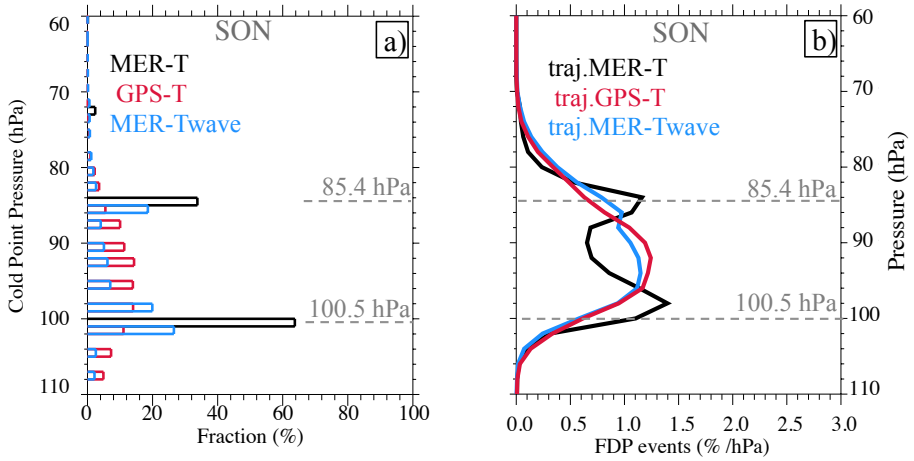

Figure 7. The relation of dehydration to cold-point tropopause during SON. **(a)** Cold-point tropopause in MERRA temperatures (black), GPS temperatures (red), and MERRA temperatures adjusted by waves (blue); and **(b)** FDP events in $\%\,hPa^{-1}$ from trajectory simulations using them. The MERRA model levels at 100.5 and 85.4 hPa are marked in dashed lines in each panel.

ACPD
14, 29209–29236, 2014

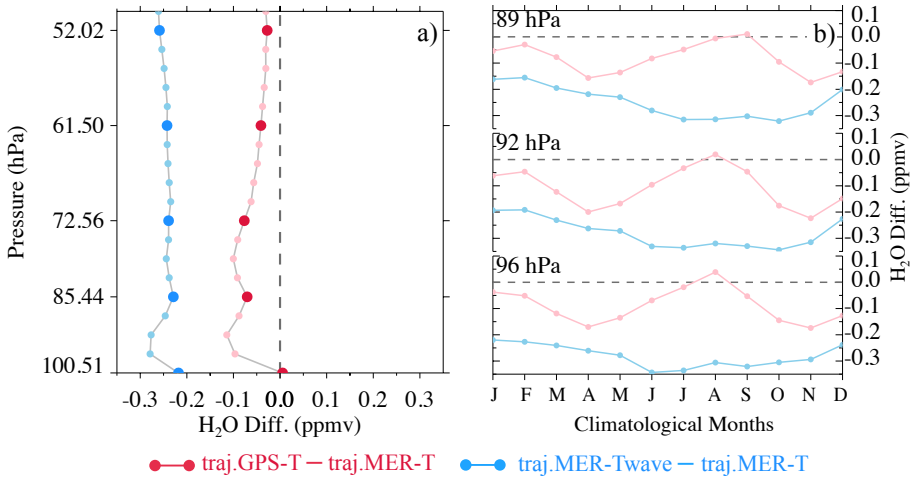

Figure 8. (a) Trajectory predicted H_2O differences induced by waves and by using GPS temperatures in the tropics (18° N–18° S). The larger dots mark the MERRA model levels and smaller dots are levels in-between MERRA model levels. **(b)** Annual differences at 96, 92, and 89 hPa. Those are the levels that the cold-point tropopause could be found but not available in MERRA model levels, so the trajectory simulations of H_2O have relatively larger biases.

ACPD
14, 29209–29236, 2014

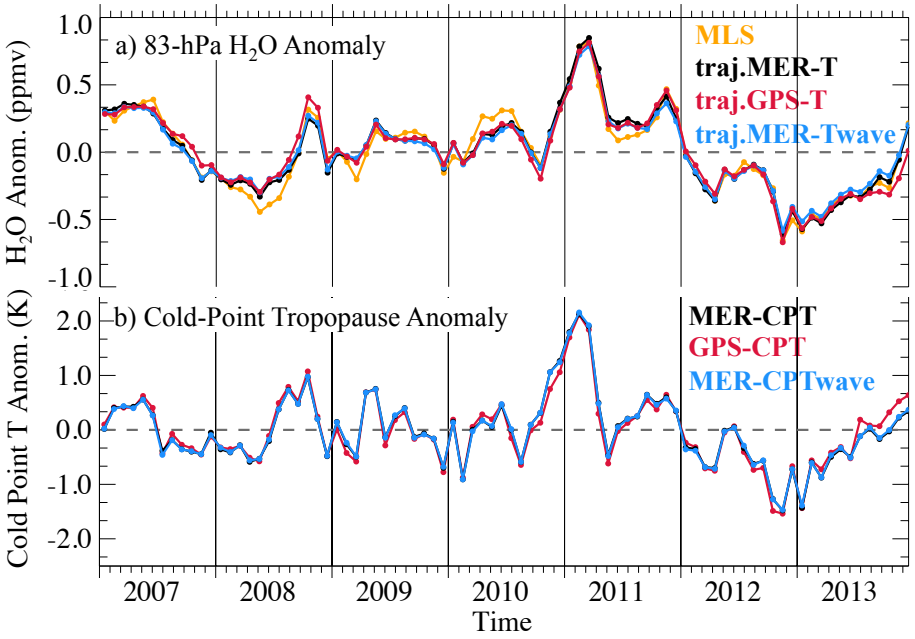

Figure 9. (a) Trajectory simulated H_2O anomalies compared with the MLS observations; and **(b)** cold-point temperature anomalies from three temperature datasets. All time series are averaged over the deep tropics (18° N–18° S). All trajectory results in panel a are weighted by the MLS averaging kernels for far comparison.

ACPD
14, 29209–29236, 2014